LETTERS
PUBLISHED ONLINE: 24 JULY 2011 | DOI: 10.1038/NMAT3076
nature materials

Seebeck effect in magnetic tunnel junctions

Marvin Walter[1], Jakob Walowski[1], Vladyslav Zbarsky[1], Markus Münzenberg[1]*, Markus Schäfers[2], Daniel Ebke[2], Günter Reiss[2], Andy Thomas[2,3], Patrick Peretzki[4], Michael Seibt[4], Jagadeesh S. Moodera[5], Michael Czerner[6], Michael Bachmann[6] and Christian Heiliger[6]

Creating temperature gradients in magnetic nanostructures has resulted in a new research direction, that is, the combination of magneto- and thermoelectric effects[1–5]. Here, we demonstrate the observation of one important effect of this class: the magneto-Seebeck effect. It is observed when a magnetic configuration changes the charge-based Seebeck coefficient. In particular, the Seebeck coefficient changes during the transition from a parallel to an antiparallel magnetic configuration in a tunnel junction. In this respect, it is the analogue to the tunnelling magnetoresistance. The Seebeck coefficients in parallel and antiparallel configurations are of the order of the voltages known from the charge–Seebeck effect. The size and sign of the effect can be controlled by the composition of the electrodes' atomic layers adjacent to the barrier and the temperature. The geometric centre of the electronic density of states relative to the Fermi level determines the size of the Seebeck effect. Experimentally, we realized 8.8% magneto-Seebeck effect, which results from a voltage change of about $-8.7\,\mu V\,K^{-1}$ from the antiparallel to the parallel direction close to the predicted value of $-12.1\,\mu V\,K^{-1}$. In contrast to the spin–Seebeck effect, it can be measured as a voltage change directly without conversion of a spin current.

The creation of an electric field by a temperature gradient in a material has been known as the Seebeck effect since 1826. In recent years new spin-dependent thermal effects have been discovered in ferromagnets and the Seebeck effect is receiving renewed interest. The transport of heat and spin in magnetic nanostructures is described in ref. 1. The spin–Seebeck effect driving this field was experimentally found, for example, in nanoscale metal structures[3] and in magnetic insulators and semiconductors[4,5]. A strong asymmetry of the density of states with respect to the Fermi level promotes the heat-driven electron transport that leads to the common charge–Seebeck effect. These strong asymmetries can be found in the spin-split density of states in ferromagnetic materials. Previously, the effect amplitude resulting from this spin asymmetry was believed to be a second-order effect. In this work, we demonstrate that the magneto-Seebeck effect can be large. We first present *ab initio* calculations that show that this effect can be of the same order as the charge–Seebeck effect, using magnetic tunnel junctions (MTJs), where two ferromagnets are separated by a thin insulating tunnel barrier. The effect is related to a half-metallic behaviour of the tunnel junction with respect to the tunnelling states. Our experiments show that a thermoelectric power can be generated in such nanostructures over distances of only 2.1 nm, the thickness of the tunnel barrier. The change from parallel to antiparallel electrode configuration is $-8.7\,\mu V\,K^{-1}$ at room temperature, while maintaining all other conditions in the junction constant. Related to this magnetization switching we calculated a magneto-Seebeck effect of 8.8%. In theory, this change is predicted to be up to $100\,\mu V\,K^{-1}$, corresponding to 1,000% (ref. 6). In future spincaloritronic[7] applications, the local cooling of an individual nanometre-sized area could, therefore, be switched magnetically. The junction size enables stacking and nano-integration of these thermopower devices.

The magneto-thermal effect is based on the seminal work described in ref. 8. This gave a general description of the mechanisms that affect a ferromagnetic material when a heat flow causes a temperature gradient. Strong thermomagnetic effects can be expected in a half-metal, where the spin polarization can be up to 100% (ref. 9). We can define a spin-dependent Seebeck coefficient by replacing the charge-dependent Seebeck voltage by a voltage generated for each spin channel. The difference between the two spin-dependent Seebeck coefficients is driving a spin accumulation. In contrast, the magneto-Seebeck effect is different from the spin–Seebeck effect, because it is not related to a spin-voltage generation. It occurs in junctions and is similar to the giant and tunnelling magnetoresistance (TMR). It results in a charge–Seebeck effect that is changed by the magnetic orientation of the electrodes. This voltage is accessible directly without conversion. To have a high charge–Seebeck effect, a high asymmetry in the energy dependence with respect to the electrochemical potential for the transport states is necessary, realized in semiconductors as shown in Fig. 1a. Consequently, for the thermomagnetic effect, these energy asymmetries must be different for spin-up and spin-down carriers. For our experiments, the recent progress in giant TMR junctions enabled us to use MTJs with high spin asymmetry. Their large contrast in the spin-dependent transmission due to different symmetries of the tunnelling states in the two spin channels should lead also to different energy asymmetries of the tunnelling states as shown in Fig. 1b. We define the magneto-Seebeck ratio (S_{MS}) from the Seebeck coefficients in the parallel (S_P) and anti-parallel (S_{AP}) configurations:

$$S_{MS} = \frac{S_P - S_{AP}}{\min(S_P, S_{AP})} \quad (1)$$

At first glance, it seems that the magnetoresistance, the spin–Seebeck effect and the magneto-Seebeck effect should be related to each other. However, these are different effects, and, in general, it is not possible to calculate one from the others.

[1]I. Physikalisches Institut, Georg-August-Universität Göttingen, 37077 Göttingen, Germany, [2]Department of Physics, Universität Bielefeld, 33501 Bielefeld, Germany, [3]Institut für angewandte Physik, Universität Hamburg, 20355 Hamburg, Germany, [4]IV. Physikalisches Institut, Georg-August-Universität Göttingen, 37077 Göttingen, Germany, [5]Massachusetts Institute of Technology, Cambridge, Massachusetts 02139, USA, [6]I. Physikalisches Institut, Justus-Liebig-Universität Gießen, 35392 Gießen, Germany. *e-mail: mmuenze@gwdg.de.

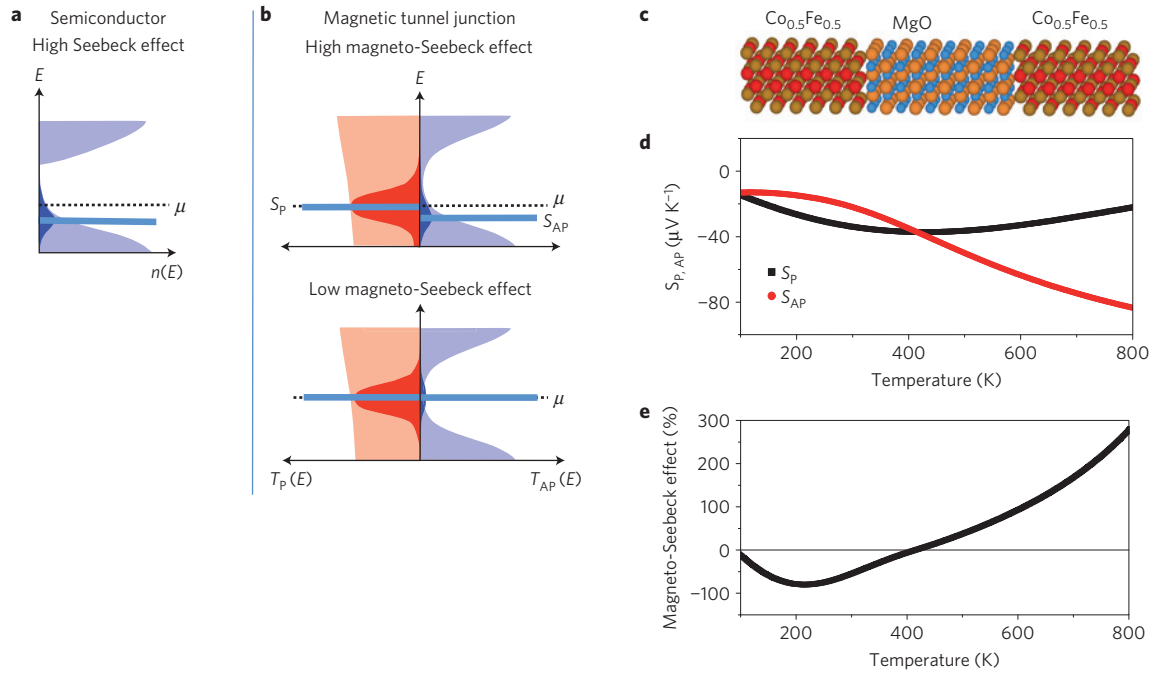

Figure 1 | Origin of the magneto-Seebeck effect. a, Semiconductors are known to generate high Seebeck effects. **b**, In MTJs, thermal differences in the electron distributions and strong asymmetry in the spin-dependent tunnelling channels are depicted. $T(E)$ is the transmission of the full tunnel junction, for which either the ferromagnetic electrodes can be a highly spin-polarized half-metal or the combination of the barrier and the ferromagnet exhibits half-metallic characteristics. The function $T(E)(-\partial_E f(E,\mu,T))$ is given in darker colour. The thick line marks the resulting value of the geometric centre S_P and S_{AP}. In the lower symmetric case, the magneto-Seebeck effect is vanishing. **c**, Calculation of the Seebeck coefficients as a function of temperature for tunnel junctions with ten monolayers of MgO as a barrier. The magnetic layers are 20 monolayers thick. The semi-infinite leads are Cu in the bcc-Fe structure. We assume a mixed termination of FeCo at the FeCo/MgO interface that is an ordered, 2×1, in-plane supercell with one Fe and one Co atom. **d**, Seebeck coefficients for the parallel configuration and the antiparallel configuration are shown. **e**, The corresponding magneto-Seebeck effect S_{MS}.

To understand this point, it is important to realize that the transport coefficients are calculated from the transmission function $T(E)$ of the tunnel junction but that they have different integral values. The conductance g is determined by the integral of the transmission function $T(E)$ multiplied by the derivative of the electron occupation function $\partial_E f(E,\mu,T)$ at temperature T and electrochemical potential μ:

$$g = \frac{e^2}{h}\int T(E)(-\partial_E f(E,\mu,T))\,\mathrm{d}E \qquad (2)$$

The Seebeck coefficient is also given by the transmission function $T(E)$ multiplied by the derivative of the occupation function $\partial_E f(E,\mu,T)$:

$$S = -\frac{\int T(E)(E-\mu)(-\partial_E f(E,\mu,T))\mathrm{d}E}{eT\int T(E)(-\partial_E f(E,\mu,T))\mathrm{d}E} \qquad (3)$$

In contrast to the magnetoresistance, the Seebeck coefficient is the geometric centre of $T(E)(-\partial_E f(E,\mu,T))$. Figure 1b illustrates these quantities for two different cases. The geometric centre for parallel and antiparallel configurations (S_P and S_{AP}) is marked by the thick line. We assume a transmission function that has different energy asymmetries in both magnetic configurations and different positions of the electrochemical potential. In the first case, a high TMR and a high magneto-Seebeck ratio are obtained. In the second case, the value of S_{MS} is essentially zero, but the TMR is highest. Generally speaking, cases with vanishing value of S_{MS} and large TMR (or vice versa) are also possible. Therefore, we can tailor MTJs to be good candidates for large magneto-Seebeck effects. Consequently, we investigated temperature-induced voltages in MTJs starting with samples showing large TMR ratios. Two different types of junction with large TMR values could be used, that is, Fe–Co/MgO/Fe–Co and half-metallic compounds. We focus on the former case, as it is demonstrated to have the largest experimental value, 604% at room temperature[10]. The tunnelling states of the electrons have been thoroughly investigated for MgO-based MTJs and the understanding of spin polarization of the current and the quantitative approach to magnetoresistance in tunnel junctions has advanced enormously in recent years.

Our theoretical investigations are *ab initio* calculations based on density functional theory. In particular, we used the Korringa–Kohn–Rostoker and the non-equilibrium Green's function method to obtain the transmission function $T(E)$ (ref. 11). Using $T(E)$, we calculated the transport coefficients according to equations (2) and (3) (refs 12,13). We investigated the magneto-Seebeck coefficients for different temperatures for $Fe_{0.5}Co_{0.5}/MgO/Fe_{0.5}Co_{0.5}$ MTJs with bcc structure of the ferromagnetic electrodes. The temperature dependence is considered only within the electron-occupation function. Owing to coherent tunnelling, the atomic structure of the interface could be important. Therefore, we investigated the Seebeck coefficients for different possible interface structures, that is, the Fe-terminated structure, the Co-terminated structure and a mixed-termination structure. The results at a temperature of 300 K listed in Table 1 show a strong dependence on the interface structure. Even a sign change was observed. However, the case where the layer next to the barrier is pure Co or pure Fe is unlikely in the experiment. Consequently, we continued our investigation with the mixed-termination structure ($Co_{0.5}Fe_{0.5}$). In Fig. 1d, S_P and S_{AP} are plotted as a function of temperature for a tunnel junction that has an MgO barrier that was 10 monolayers thick. In addition, we plot the corresponding magneto-Seebeck ratios (Fig. 1e). Although S_P and S_{AP} do not change sign, S_{MS} does when

Table 1 | The Seebeck coefficients for parallel S_P and antiparallel S_{AP} configurations and the magneto-Seebeck effects calculated for different supercells at a temperature of 300 K.

FeCo/MgO/FeCo with a ten-monolayer MgO barrier

	S_P (μV K^{-1})	S_{AP} (μV K^{-1})	$S_P - S_{AP}$ (μV K^{-1})	S_{MS} (%)
CoFe	−19.7	−32.4	12.7	64.1
FeCo	45.9	−50.0	95.9	209.0
CFFC	9.4	−44.6	54.0	573.2
$Co_{0.5}Fe_{0.5}$	−34.0	−21.9	−12.1	−55.2
Experimental value	−107.9 (−1,300)	−99.2 (−1,195)	−8.7 (−105)	−8.8 (−8.8)

The results show the sensitivity to the interface composition. S_{MS} defines the relative change and can be negative or positive. Abbreviations: CoFe—$Co_{0.5}Fe_{0.5}$ layers with Co at the MgO interface. FeCo—$Co_{0.5}Fe_{0.5}$ layers with Fe at the MgO interface. CFFC—$Co_{0.5}Fe_{0.5}$ layers with Fe at one of the MgO interfaces and Co at the other. $Co_{0.5}Fe_{0.5}$—supercell in plane with Co:Fe 1:1 at the interface. The values derived from the experiment are given for a temperature difference at the MgO barrier of 53 mK (4.4 mK) respectively. The temperature difference ΔT is taken from the numerical simulation of the temperature gradients using the thin-film value (bulk value) of the thermal conductivity of MgO.

$S_P = S_{AP}$. We found that S_P and S_{AP} were large when compared with charge–Seebeck coefficients.

For the experiments, we use Co–Fe–B/MgO/Co–Fe–B pseudo-spin-valve structures. The $1 \times 1\,\mu m^2$ tunnel junction is heated homogeneously by 30 mW laser power (diode laser with 15–20 μm focus in diameter and a wavelength of 784 nm, Fig. 2a,b) and the charge–Seebeck voltage (Seebeck voltage in the following) is measured for the parallel and antiparallel orientations of the layer magnetization (Fig. 2c,d). To obtain the temperature distribution and the time constants for the heat diffusion, we used finite-element simulations. Transmission electron microscopy (TEM) in Fig. 3a reveals the device geometry that serves as an input to integrate the heat diffusion equation. To calculate the Seebeck coefficients, we estimate a temperature difference ΔT at the 2.1 nm MgO barrier. For polycrystalline MgO films with a nanometre grain size, the heat conductance is lower than the bulk value owing to the grain boundaries[14]. The high-resolution TEM in Fig. 3a, however, reveals a good crystalline quality of the investigated samples. Nevertheless, the thermal resistance at the Co–Fe/MgO interfaces can have similar effects to the grain boundaries. Therefore, we used both the bulk and the reduced value for the thermal conductivities as given in Supplementary Information.

In Fig. 3b we show the resulting temperature profile in a two-dimensional cross-section for 200 ps and 1 μs after the laser power is turned on. A series enables determination of the timescales of the heating: the static temperature profile is reached after about 2 μs. The final temperature distribution is shown as a line scan in Fig. 3c across the tunnel junction. A temperature difference at the 2.1 nm MgO barrier of 53 mK (4.4 mK) is derived from the numerical simulation using the thin-film value (bulk value) of the thermal conductivity of MgO respectively.

Figure 4 shows the magneto-Seebeck effect of a single MTJ with a TMR of 150%. The temporal voltage traces in Fig. 4a, as observed in several junctions, show a peak-like voltage when the laser heating is increased and decreased periodically. A negative peak occurs when the laser power is turned on. From the time constants simulated we identify this voltage peak with the Seebeck voltage generated at the junction. The shutter moving through the laser spot limits the timescale to approximately 10–100 μs in our data. As a reference the sequence of the measured laser power is given for each signal trace. The voltage reverses sign when the laser heating is turned off. The Au pads efficiently conduct the heat away from the heat spot (extension of 17.5 μm) into the large bond pads that act as a heat sink. The other side of the junction is then still at a higher temperature and the temperature gradient is reversed. In the lowest curve with an 800 Hz modulation frequency, the MTJ was heated asymmetrically, enabling a longer cooling time. The Seebeck voltages for the parallel and antiparallel configurations are determined from Fig. 4b, in which the Seebeck voltage is shown as a

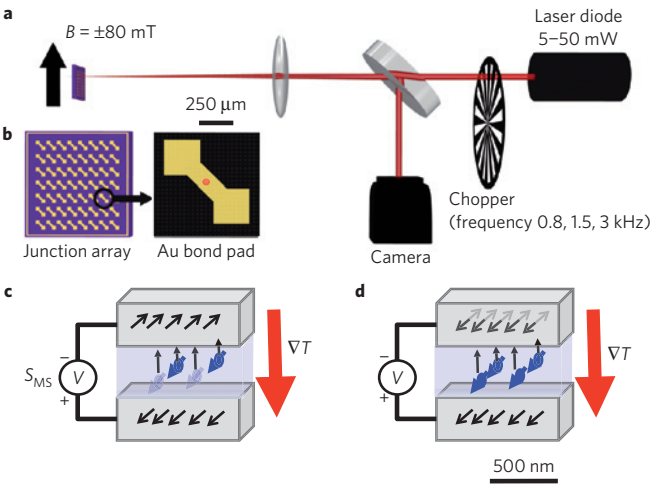

Figure 2 | Switching of the Seebeck effect through the magnetization. **a**,**b**, Schematic representations of the laser-heating set-up (**a**) and the Au top-contact geometry of the device with the laser spot dimensions (**b**). **c**,**d**, From antiparallel (**c**) to parallel (**d**) orientation of the layer magnetization, the charge–Seebeck voltage varies. By the magnitude of its change the magneto-Seebeck effect S_{MS} is defined.

function of the applied field. As expected from the temporal traces, a larger value was found for the fastest modulation of the laser power (at 3 kHz). The Seebeck voltage at the junction contributes more to the total signal than it does for the slower modulation, where the whole sample heats up on a larger area. A signal proportional to the modulation frequency is the dominant component. We obtain −5.7 μV for the parallel and −5.3 μV for the antiparallel orientation, that is, a change of the Seebeck voltage by 0.4 μV for the tunnel junction. Fluence-dependent experiments suggest that the increase of the Seebeck voltage with laser power depends on the increase of the temperature gradient at the barrier and the base temperature at the junction, which is increased by the laser power as well, as discussed further in Supplementary Information. If the junction barrier is pushed through a dielectric breakdown[15], the magneto-Seebeck effect disappears.

The experimental results and the theoretical predictions for the Seebeck coefficients are summarized in Table 1. The theoretical prediction for the $Co_{0.5}Fe_{0.5}$ case with Co:Fe 1:1 at the interface is closest to the experiment. The values are negative for both the parallel and the antiparallel configuration. To calculate the Seebeck coefficients from the experimentally determined Seebeck voltage $V_{P,AP}$, we take the temperature gradient to be 53 mK across the 2.1 nm MgO tunnel barrier from our numerical modelling. Thus, we obtain a value of $V_P/\Delta T = -108\,\mu V\,K^{-1}$ for the Seebeck

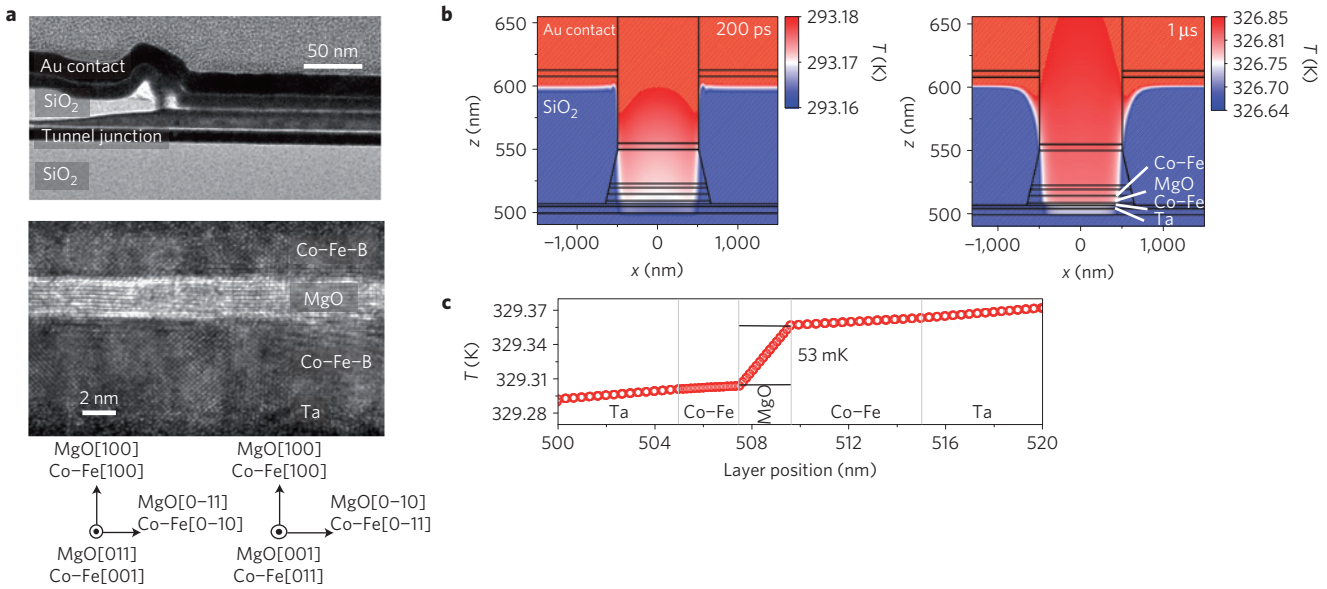

Figure 3 | Cross-sections and temperature gradients in the tunnel junction. a, TMR junctions: device structure studied with TEM. The high resolution shows the epitaxial relationship Fe-Co(001)/MgO(001) for two transmission directions, MgO[100] and MgO[110]. **b**, The simulated temperature distributions for 200 ps and 1 µs after the laser power of 30 mW is turned on in a two-dimensional cross-section. **c**, The temperatures for the final static-equilibrium condition as a line scan.

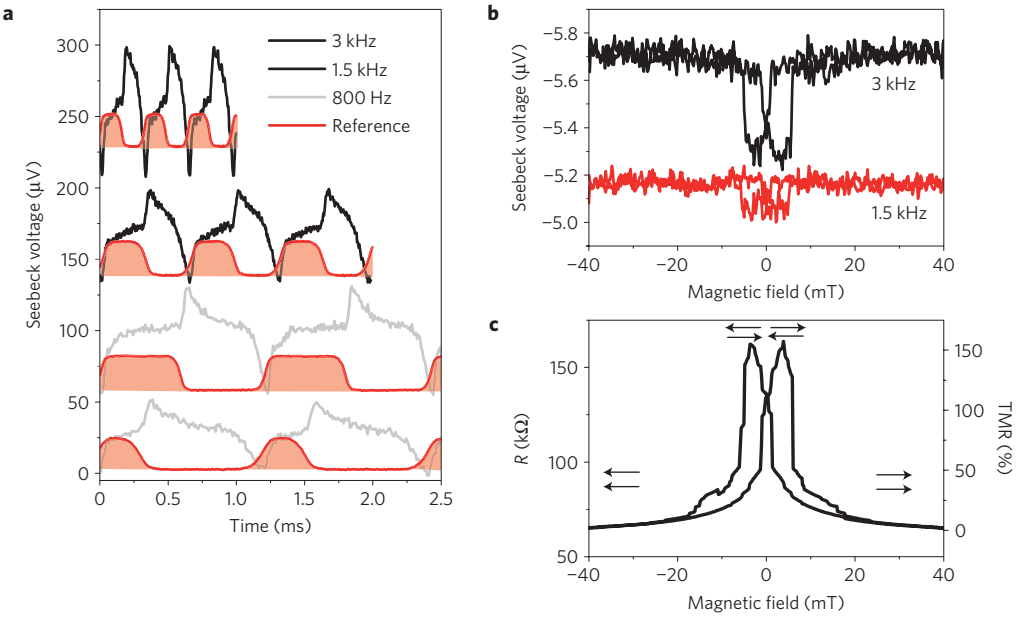

Figure 4 | Seebeck voltages for Fe-Co-B/MgO/Fe-Co-B elements. a, Temporal traces are shown for different modulation frequencies. The heating by the laser is shown in red overlaid on the corresponding Seebeck voltage (the voltages are shifted for clarity). **b**, Magneto-Seebeck voltages are given above for 1.5 and 3 kHz lock-in modulation. **c**, The corresponding magnetoresistance (TMR) shows a hard–soft switching of the pseudo-spin-valve structure.

coefficient S_P for the parallel orientation. A decrease of the thermal gradient taking the bulk value for the MgO thermal conductivity as input parameter in our model increases the Seebeck coefficients calculated accordingly. This enables derivation of an upper limit of $-1{,}300\,\mu V\,K^{-1}$ for the Seebeck coefficient, given in brackets. Note that spurious other voltages generated in the layer stacks or within the heated device change the Seebeck-effect amplitude, but not the difference of the Seebeck voltage for parallel and antiparallel configurations. In accordance with this, the experimental results for the difference $(S_P - S_{AP})$ of $-8.7\,\mu V\,K^{-1}$ are closer to the predicted value of $-12.1\,\mu V\,K^{-1}$ than the individual values of S_P and S_{AP}. The lower limit of the magneto-Seebeck effect, that is, the relative change of the Seebeck voltage for the parallel and the antiparallel case, is −8.8%.

Finally, the magneto-Seebeck effect in MTJs enables control of these effects. As a major strategy to develop the possibilities opening up with the magneto-Seebeck effect it is crucial to tailor the thermal tunnelling current arising from the majority and the minority spins, that is, to maximize the shift of the geometric centre relative to the Fermi level of these electronic states contributing to the thermal transport. The calculations demonstrate that even the sign of the magneto-Seebeck effect can be controlled using different Co–Fe compositions. Findings on tunnel junctions using a different method (resistive heating) yielding the same effect

magnitudes with different sign were recently reported[16] using Co–Fe–B/MgO/Co–Fe–B devices but of different composition and structure (using a Singulus Tech. cluster tool). The qualitative change for the devices presented here however enables comparison of theoretical and experimental results. The results presented compare well to the theoretically predicted change, including the predicted sign reversal of the magneto-Seebeck effect at elevated temperatures (see Supplementary Information). Further, the experiments showed that the magneto-Seebeck effect can be generated over length scales of only a few nanometres—across a 2.1-nm-thick tunnel barrier in our case. This reveals that the magneto-Seebeck effect in MTJs can be used to manipulate and design thermovoltages in nanometre-scale devices. The contrast for switching the voltage can be increased further in the future, which will enable control of the Seebeck effect by magnetic switching.

Note added in proof. After acceptance of this paper, we became aware of a paper by Jansen and colleagues[17] demonstrating a thermal injection of spins from a ferromagnet through an Al_2O_3 tunnel barrier into silicon.

Methods

Fabrication. The Co–Fe–B films were prepared by magnetron sputtering using 2 inch targets with compositions of $Co_{0.4}Fe_{0.4}B_{0.2}$ (analysis Co:Fe 0.52:0.48) and $Co_{0.2}Fe_{0.6}B_{0.2}$ (analysis Co:Fe 0.32:0.68) in an ultrahigh-vacuum system with a base pressure of 5×10^{-10} mbar. They are annealed *ex situ* at temperatures of 450–550 °C (post-growth annealing, 20–60 min). For samples prepared in the Göttingen chamber MgO was e-beam evaporated after transferring to a separate ultrahigh-vacuum chamber with base pressure of 5×10^{-10} mbar (maximum TMR reached is 200% at room temperature). With the Bielefeld chamber, MgO was prepared by magnetron sputtering (maximum TMR reached is 330% at room temperature). The sample stack was reduced to a simple pseudo-spin-valve structure to minimize the contribution of spurious Seebeck voltages at metal interfaces not stemming from the junction: Au 27 nm/Ru 3 nm/Ta 5 nm/Co–Fe–B 5.4 nm/MgO 2.1 nm/Co–Fe–B 2.5 nm/Ta 5 nm/SiO_2 500 nm/Si(100). This was done as a trade-off with the magnetic separation of the switching fields, because no antiferromagnetic exchange-bias layer is used, which could also give a magnetic contribution. After *ex situ* annealing in a constant field, further structuring was done by standard ion-beam etching to yield $1 \times 1\,\mu m^2$ to $12.5 \times 12.5\,\mu m^2$ junctions to the MgO barrier. The high-resolution TEM data in Fig. 3 (bottom, left) reveal the coherent growth of crystallized Co–Fe(110) on each side of the MgO(100) barrier (solid-state epitaxy) in columns that can be identified (MgO[001] and MgO[110] in the transmission direction). As an isolation layer at the sides of the element, a 100-nm-thick SiO_2 layer was grown by thermal evaporation. A 100-nm-thick, top-contact Au layer was deposited as a bond pad. This also prevents direct optical carrier excitation in the MgO barrier. A 5 nm layer of Cr was deposited below the Au top-contact layer for better adhesion on the SiO_2 isolation.

Experimental set-up. For the laser heating, a 100 mW, Toptica, intensity-stabilized laser diode module (wavelength, $\lambda = 784$ nm) was focused to a diameter of 15–20 μm full-width at half-maximum. For the standard experiments we used 30 mW laser power. The beam position on top of the bond pad was controlled through a camera. The intensity was modulated using 800 Hz, 1.5 kHz and 3 kHz modulation frequencies. To prevent a current flow in the system that could be modified by the change of the resistance of the junction, a high-input-impedance (100 GΩ) LT1113 precision operational amplifier (Linear Technology) was used. The bandwidth of the amplifier is 5 MHz. This was installed close to the sample to minimize the effect of the cable capacitance (<15 pF). A simulation of the circuit with the sample resistance showed that the change of the resistance will contribute <1 nV to the absolute voltage. Curves of Seebeck voltage versus magnetic field are measured using a Stanford Linear Research lock-in amplifier.

Thermal modelling of parameters (COMSOL). To simulate heat flow and temperature distribution, the MTJ was modelled using the COMSOL finite-element package. The tunnel-junction geometry was taken from the cross-sectional TEM data as input parameters. The element was embedded into a 3 μm cylinder. The heat flow from the laser heating comes from the top. For a 30 mW laser power the absorbed laser power is 10 mW. The temperature at the bottom of the cylinder in the Si(100) substrate was set to ambient temperature. The 500 nm SiO_2 layer on top of the substrate is the bottleneck for heat diffusion through the cylinder stack. The temperature at the bottom layer of the element depends sensitively on the heat flow though the SiO_2 layer and determines the 2 μs needed to reach the final heat gradient. A prism-shaped, adaptive mesh was used with resolution >10 nm in the plane and subnanometre perpendicular to the plane. In addition, we carried out simulations on a larger length scale to simulate lateral heat diffusion. The heated area extends to about 17.5 μm diameter, and, in this case, the absolute temperature increase is reduced to 8 K. The equilibrium heat gradient is attained within about 2 μs. For the 2.1 nm MgO thin tunnel barrier, a value of the thermal conductance of $\kappa = 4\,W\,(mK)^{-1}$ is assumed to be closest to reality. This value has been determined experimentally for a thin film[14]. It is expected to be much closer to the bulk value of $\kappa = 48W\,(mK)^{-1}$, which gives an upper limit for the Seebeck coefficient. All material parameters used in the numerical model are provided in a table in Supplementary Information.

Received 14 February 2011; accepted 20 June 2011; published online 24 July 2011

References

1. Gravier, L., Serrano-Guisan, S., Reuse, F. & Ansermet, J. P. Thermodynamic description of heat and spin transport in magnetic nanostructures. *Phys. Rev. B* **73,** 024419 (2006).
2. Uchida, K. *et al.* Observation of the spin–Seebeck effect. *Nature* **455,** 778–781 (2008).
3. Slachter, A., Bakker, F. L., Adam, J. P. & van Wees, B. J. Thermally driven spin injection from a ferromagnet into a non-magnetic metal. *Nature Phys.* **6,** 879–882 (2010).
4. Uchida, K. *et al.* Spin Seebeck insulator. *Nature Mater.* **9,** 894–897 (2010).
5. Jaworski, C. M., Yang, J., Awschalom, D. D., Heremans, J. P. & Myers, R. C. Observation of the spin-dependent Seebeck effect in a ferromagnetic semiconductor. *Nature Mater.* **9,** 898–903 (2010).
6. Czerner, M., Bachmann, M. & Heiliger, C. Spin caloritronics in magnetic tunnel junctions: *Ab initio* studies. *Phys. Rev. B* **83,** 132405 (2011).
7. Bauer, G. E. W., MacDonald, A. H. & Maekawa, S. Spin caloritronics. *Solid State Commun.* **150,** 459–460 (2010).
8. Johnson, M. & Silsbee, R. H. Thermodynamic analysis of interfacial transport and of the thermomagnetoelectric system. *Phys. Rev. B* **35,** 4959–4972 (1987).
9. Müller, G. *et al.* Spin polarization in half metals probed by femtosecond spin excitation. *Nature Mater.* **8,** 56–61 (2009).
10. Ikeda, S. *et al.* Tunnel magnetoresistance of 604% at 300 K by suppression of Ta diffusion in CoFeB/MgO/CoFeB pseudo-spin-valves annealed at high temperature. *Appl. Phys. Lett.* **93,** 082508 (2008).
11. Heiliger, C., Czerner, M., Yu, Yavorsky, B., Mertig, I. & Stiles, M. D. Implementation of a non-equilibrium Green's Function Method to calculate spin transfer torque. *J. Appl. Phys.* **103,** 07A709 (2008).
12. Sivan, U. & Imry, Y. Multichannel Landauer formula for thermoelectric transport with application to thermopower near the mobility edge. *Phys. Rev. B* **33,** 551–558 (1986).
13. Ouyang, Y. & Guoa, J. A theoretical study on thermoelectric properties of graphene nanoribbons. *Appl. Phys. Lett.* **94,** 263107 (2009).
14. Lee, S. M., Cahill, D. G. & Allen, T. H. Thermal conductivity of sputtered oxide films. *Phys. Rev. B* **52,** 253–257 (1995).
15. Thomas, A. *et al.* Direct imaging of the structural change generated by dielectric breakdown in MgO based magnetic tunnel junctions. *Appl. Phys. Lett.* **93,** 152508 (2008).
16. Liebing, N. *et al.* Tunnelling magneto thermo power in magnetic tunnel junction nanopillars. Preprint at http://arxiv.org/abs/1104.0537 (2011).
17. Le Breton, J-Ch., Sharma, S., Saito, H., Yuasa, S. & Jansen, R. Thermal spin current from a ferromagnet to silicon by Seebeck spin tunnelling. *Nature* **475,** 82–85 (2011).

Acknowledgements

A.T. acknowledges the Ministry of Innovation, Science and Research of the North Rhine-Westphalia state government for financial support. M.M., M.S., M.W. and P.P. acknowledge the funding provided by the German Research Foundation through the SFB 602 for the TEM work. M.C., M.B. and C.H. acknowledge support from German Research Foundation SPP 1386 and German Research Foundation grant HE 5922/1-1. J.S.M acknowledges support by the US National Science Foundation and Office of Naval Research. We acknowledge A. Zeghuzi's help for extra COMSOL calculations. This work was initiated by the SpinCaT priority program.

Author contributions

M.W. and J.W. carried out experiments; M.W., V.Z., M.Sch. and D.E. characterized and prepared the TMR devices; P.P. and M.S. carried out the high-resolution TEM; M.W., J.W. and M.M. analysed the data; M.W. carried out the COMSOL calculations; M.C., M.B. and C.H. did the *ab initio* transport calculations; A.T. and M.M. designed the research approach; C.H., M.M. and A.T. wrote the manuscript and developed the model; M.W., J.S.M., A.T., M.M. and C.H. contributed to the development of the experiments; G.R., J.S.M., A.T., M.M., C.H. and all authors discussed the experiments and the manuscript.

Additional information

The authors declare no competing financial interests. Supplementary information accompanies this paper on www.nature.com/naturematerials. Reprints and permissions information is available online at http://www.nature.com/reprints. Correspondence and requests for materials should be addressed to M.M.